Long-range chromatin interactions at the mouse Igf2/H19 locus reveal a novel paternally expressed long non-coding RNA

Franck Court, Marion Baniol, Hélène Hagège, Julie Sandrine Petit, Marie-Noëlle Lelay-Taha, Françoise Carbonell, Michael Weber, Guy Cathala, Thierry Forné

Published online 7 April 2011

Nucleic Acids Research, 2011, Vol. 39, No. 14 ***5893–5906***
doi:10.1093/nar/gkr209

Long-range chromatin interactions at the mouse *Igf2/H19* locus reveal a novel paternally expressed long non-coding RNA

Franck Court, Marion Baniol, Hélène Hagege, Julie Sandrine Petit, Marie-Noëlle Lelay-Taha, Françoise Carbonell, Michael Weber, Guy Cathala and Thierry Forne*

Institut de Génétique Moléculaire de Montpellier, UMR5535 CNRS Universités Montpellier I et Montpellier II, 1919 Route de Mende, 34293 Montpellier cedex 5, France

Received October 22, 2010; Revised March 21, 2011; Accepted March 23, 2011

ABSTRACT

Parental genomic imprinting at the *Igf2/H19* locus is controlled by a methylation-sensitive CTCF insulator that prevents the access of downstream enhancers to the *Igf2* gene on the maternal chromosome. However, on the paternal chromosome, it remains unclear whether long-range interactions with the enhancers are restricted to the *Igf2* promoters or whether they encompass the entire gene body. Here, using the quantitative chromosome conformation capture assay, we show that, in the mouse liver, the endodermal enhancers have low contact frequencies with the *Igf2* promoters but display, on the paternal chromosome, strong interactions with the intragenic differentially methylated regions 1 and 2. Interestingly, we found that enhancers also interact with a so-far poorly characterized intergenic region of the locus that produces a novel imprinted long non-coding transcript that we named the paternally expressed *Igf2/H19* intergenic transcript (*PIHit*) RNA. *PIHit* is expressed exclusively from the paternal chromosome, contains a novel discrete differentially methylated region in a highly conserved sequence and, surprisingly, does not require an intact ICR/*H19* gene region for its imprinting. Altogether, our data reveal a novel imprinted domain in the *Igf2/H19* locus and lead us to propose a model for chromatin folding of this locus on the paternal chromosome.

INTRODUCTION

The imprinted *IGF2/H19* locus plays a causative role in several embryonic growth disorders and various cancers. The *insulin-like growth factor 2 (Igf2)* gene is expressed exclusively from the paternal chromosome during embryonic development. The *H19* gene is maternally expressed and produces an untranslated RNA which was recently shown to act in mice as a *trans*-regulator (1) of the imprinted gene network controlling embryonic growth (2). Imprinting of both genes is depending on an imprinting-control region (ICR), which acquires DNA methylation during male germ-cell development and is therefore differentially methylated in the embryos. Binding of the CCCT C binding factor (CTCF) to the unmethylated maternal ICR creates an insulator (3) that prevents downstream enhancers from accessing the *Igf2* gene, thus maintaining silencing of the *Igf2* maternal allele. On the paternal chromosome, CTCF cannot bind to the methylated ICR and *Igf2* can thus interact with the enhancers (4,5). Furthermore, two differentially methylated regions (DMRs), which are preferentially methylated on the paternal chromosome (6) play important roles in expression and imprinting of the *Igf2* gene in the embryo. The DMR1 acts as an *Igf2* silencer involved in imprinting on the maternal allele and post-natal repression on the paternal allele (7), while the intragenic DMR2 augments *Igf2* transcription on the paternal allele (8).

3C experiments [reviewed in Ref. (9)] combined with an elegant transgenic model (10) showed that at the mouse *Igf2/H19* locus the parental chromosomes adopt distinct high-order chromatin conformations and that CTCF play a central role in the formation of chromatin loops. On the maternal chromosome, the ICR/CTCF insulator interacts with both the *Igf2* DMR1 and a matrix attachment region (MAR3) (10,11). Subsequent studies provided evidence that the enhancers and proximal *Igf2* promoters can be detected in close spatial proximity with the maternal ICR (12) and that, in epithelial human cells, these interactions are dependent on the cohesin protein (13), which was known to co-localize with CTCF (14–17). Overall, these

*To whom correspondence should be addressed. Tel: +33 467 61 36 84; Fax: +33 467 04 02 31; Email: thierry.forne@igmm.cnrs.fr

results are strengthening a consensus model for chromatin folding at the *Igf2/H19* locus on the maternal chromosome (11).

The picture is less clear for chromatin folding on the paternal chromosome. In human, chromatin folding appears to rely on interactions between CTCF/cohesin sites that bring the enhancers close to the *IGF2* gene (18). However, it remains unclear whether the contacts are preferentially made with the promoters (19) or whether they encompass the entire gene body (11,20). To elucidate this point, we performed 3C-qPCR assays (20) on mouse liver samples to examine interaction frequencies between the endodermal enhancers and the entire *Igf2/H19* locus. Our results identified paternal-specific contacts with the *Igf2* DMR1 and DMR2, which are preferentially methylated on the paternal chromosome (6,21), and no significant interactions with the *Igf2* promoters. Moreover, the identification of an unexpected interaction with a poorly characterized intergenic region of the locus led us to discover a novel imprinted domain producing an untranslated RNA that we called the paternally expressed *Igf2/H19* intergenic transcript (*PIHit*). Overall, our data suggest a novel model for chromatin folding at the *Igf2/H19* locus on the paternal chromosome.

MATERIALS AND METHODS

Ethics statement

All experimental designs and procedures are in agreement with the guidelines of the animal ethics committee of the French 'Ministère de l'Agriculture'.

Mouse strains

Mice carrying genomic deletions were maintained as homozygous strains. For embryo collection, matings were performed to produce plugs and the day of plug was considered as e0.5. The *SDP711* strain used in this work is a congenic mouse strain where the distal part of chromosome 7 and the proximal part of chromosome 11 are of *Mus spretus* origin.

3C-qPCR/SybGreen

The 3C-qPCR assays were performed as previously described (20) with a few important modifications. First, the presence of ATP during the enzymatic digestion (Steps 10–13) increases significantly digestion efficiencies. Second, incubating at 37°C, instead of 65°C, at Step 16 (SDS inactivation of the restriction enzyme) prevents decrosslinking before the ligation step. These modifications increased four times the efficiency of 3C assays thus allowing real-time PCR quantifications of 3C products by the SybGreen technology in replacement of TaqMan probes used in previous works (20,22). Detailed modifications are as follow: Step 2: 5×10^6 nuclei were cross-linked at 1% formaldehyde. Step 8: add 5 µl of 20% (w/v) SDS (final: 0.2%). Step 10: add 50 µl of 12% (v/v) Triton X-100 diluted in 1× ligase buffer from Fermentas (40 mM Tris–HCl pH 7.8; 10 mM $MgCl_2$; 10 mM DTT; 5 mM ATP). Step 13: add 450 U of restriction enzyme (here BamHI was used). Step 16: incubate 30 min at 37°C; shake at 900 rpm. Step 34: additional digestions were performed using EcoRI. Step 39: adjust 3C assays with H_2O to 25 ng/µl. 3C products were quantified on a LightCycler 480 II apparatus (Roche) (10 min at 95°C followed by 45 cycles 10 s at 95°C/8 s and 69°C/14 s at 72°C) using the Hot-Start Taq *Platinium* Polymerase from Invitrogen (10966-34) and a standard 10× qPCR mix (23) where the usual 300 µM dNTP have been replaced by 1500 µM of CleanAmp dNTP (TEBU 040N-9501-10). Standard curves for qPCR have been generated from the RP23 BAC (Invitrogen) as previously described (20). The sequence of primers used for qPCR quantification of 3C products are given in Supplementary Table S1.

For each biological sample, a Basal Interaction Level (BIL) was calculated and 3C-qPCR data were normalized to this BIL as previously described (22). Briefly, we first calculate the mean interaction frequency (*M*) and the mean standard deviation (SD) of all the experimental points. Experimental points are selected if their interaction frequency (*fx*) is both superior to (Mean − SD) and inferior to (Mean + SD). The mean *fx* of the selected experimental points is corresponding to the 'BIL' to which all *fx* values of the experiment are normalized. For a detailed procedure please refer to our previous publication (22).

RNA preparation and northern blots

Preparations of total RNAs were as previously described (24) and polyadenylated RNAs were purified by using the PolyA Tract mRNA isolation system III® (Promega). Nuclear RNAs were prepared similarly from purified nuclei (24). The *Igf2* and intergenic probes used in northern blots are PCR products obtained by amplification of genomic DNA. PCR primer sequences are available in Supplementary Table S3. The *Igf2* probe is located in the exon 6 which is common to all *Igf2* mRNA transcripts.

RT–qPCR: random priming/ssRT–PCR/allele-specific PCR

cDNA were produced by reverse transcription of total RNA preparations by the Superscript III® RT enzyme (Invitrogen, ref. 18 080). RT products were quantified in capillary tubes on a LightCycler apparatus (Roche) (3 min at 95°C followed by 45 cycles 0.5 s at 95°C/5 s at 70°C/15 s at 72°C) using the Hot-Start Taq Platinium® Polymerase from Invitrogen (ref. 10966-34) and a standard 10× qPCR mix (23). Primer sequences are given in Supplementary Tables S2, S4 and S8.

Rapid amplification of 5′ complementary DNA ends

Rapid amplification of 5′ complementary DNA ends (5′-RACE) was performed according to manufacturer's instructions (GeneRacer® Kit from *Invitrogen* ref. L1502). 5′-RACE PCR Primer sequences are given in Supplementary Table S7.

Genomic HRS assays

Genomic high-salt recovered sequence (HRS) assays were performed as previously described (25). High-concentration restriction enzymes were purchased from Fermentas. The sequences of qPCR primers used for quantifications of genomic DNA in the loop and HRS fractions are given in Supplementary Tables S5 and S6.

Bisulphite treatments

Genomic DNA was prepared from livers of 7-days-old hybrid mice issued from matings between *Mus musculus domesticus* females with *SDP711* males and from the reverse cross. Conversion with sodium bisulphite was performed with the Epitect® kit (Qiagen) following the manufacturer's instructions. PCR fragments were cloned using a PCR cloning Kit from Qiagen. Clones with strictly identical patterns of conversion were removed from the results (since they are likely to represent identical molecules). We used the MethPrimer software to design primers on bisulphite treated DNA. Primer sequences are given in Supplementary Table S9.

Allele-specific methylation analysis

Methylation levels of the HRS2 region were determined on genomic DNA samples from *M. musculus domesticus* X *SDP711* hybrid mice. Each sample was digested by the BamHI and BglII restriction enzymes (20 U each) to eliminate potential PCR bias due to the reduced accessibility of primers on undigested genomic DNA (26). Half of each samples was then additionally digested by the BceAI methylation-sensitive enzyme (20 U/reaction) and qPCR quantifications, using allele specific primers, were performed on BceAI-digested and undigested fractions. Primer sequences are available in Supplementary Table S10.

URLs

UCSC genome annotation: http://www.genome.ucsc.edu; MethPrimer software: http://www.urogene.org/methprimer/index1.html; MAR-Wiz 1.5 software: http://www.futuresoft.org.

RESULTS

The endodermal enhancers interact with the *Igf2* DMRs and an intergenic region

To determine the interaction frequencies of the endodermal enhancers throughout the *Igf2*/*H19* locus, we used an improved version (see 'Materials and Methods' section) of the sensitive 3C-qPCR method (20) and applied our algorithm that helps to define the level of background interactions and normalize 3C assays from diverse biological samples (22). 3C-qPCR assays were performed on the 7-days-old mouse liver, which is the period that displays the highest *Igf2* and *H19* gene expression levels (27,28), and interaction frequencies were determined between BamHI site 0 (Anchor), located 3.9 kb downstream from the endodermal enhancers, and the others BamHI sites of the locus (Sites 1–21) (Figure 1). As observed previously (22), high-interaction frequencies of sites separated by <35 kb from the 'anchor' reflect close physical proximity ('side effect' in Figure 1) and are not considered specific. In the 7-days-old mouse liver, the endodermal enhancers were found to specifically interact with four genomic sites (Sites 19, 16, 12 and 10 in Figure 1) that were identified as 'local peaks' above the noise band (horizontal grey bars in Figure 1). Sites 19 and 16 correspond to the DMR1 and DMR2, respectively, while Sites 12 and 10 are located in a poorly characterized intergenic region. Interaction frequencies observed with the rest of the locus were close to the background of unspecific random collisions (noise band) and, noticeably, contacts observed with the *Igf2* promoter P1 and P2/P3 (Sites 18 and 17, respectively) were very low. Interestingly, interactions with Sites 19, 16 and 10 are lost in the 30-days-old mouse liver (Figure 1, black diamonds), when the *Igf2* and *H19* genes become fully repressed (27,28), suggesting a functional relationship between these contacts and gene expression at this locus. We thus decided to focus our experiments on these three interactions.

The enhancers/*Igf2* DMRs interactions are specific of the paternal chromosome

To determine on which parental allele the enhancers/DMRs interactions occur, we analysed samples from 7-days-old mouse livers issued from strains carrying DMR deletions. Compared to wild-type control mice (Figure 2, white circles), the enhancers/DMR1 interaction (Site 19) is lost upon paternal inheritance of the ΔDMR1-U2 deletion (7) (Figure 2B, grey triangles). We conclude that, in the 7-days-old mouse liver, the *H19* endodermal enhancers interact with the *Igf2* DMR1 on the paternal chromosome. Interestingly, the interaction with the DMR2 (Site 16) is also lost upon paternal inheritance of the DMR1 deletion, indicating that this interaction depends on an intact DMR1 sequence. Conversely, maternal inheritance of the ΔDMR1-U2 deletion has no significant effect on the enhancers/DMRs interactions (Figure 2C), indicating that the enhancers/DMR1 interaction occurs exclusively on the paternal allele. We then used ΔDMR2 mouse mutants (8) and showed that, upon paternal transmission of this deletion, the enhancer/DMR2 interaction is abolished (Figure 2D). We conclude that the enhancer/DMR2 interaction also occurs on the paternal chromosome. Interestingly, the interaction with DMR1 remains intact, suggesting that DMR2 is dispensable for the enhancer/DMR1 interaction. Finally, in both deletions, the interaction with the intergenic Site 10 is moderately affected and loss of enhancer/DMR interactions results in a drastic reduction of *Igf2* mRNA levels (Supplementary Figure S1A).

The enhancers/*Igf2* DMRs interactions depend on an intact ICR/*H19* gene region

We then analysed interaction frequencies in the context of the H19Δ13 deletion, which removes the ICR and the entire *H19* gene region (29). This deletion leads to biallelic *Igf2* expression and loss of *H19* expression when maternally (29). Upon maternal inheritance, we observed that

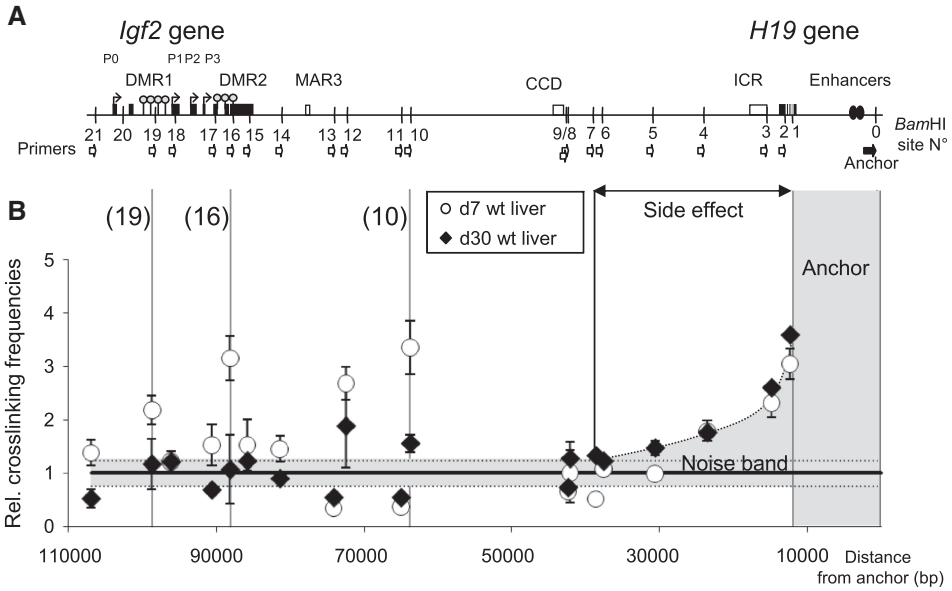

Figure 1. Long-range interactions with endodermal enhancers at the *Igf2*/*H19* locus in the mouse liver. (**A**) Schematic representation of the mouse *Igf2*/*H19* locus. Exons of the *Igf2* and *H19* genes (black boxes) are displayed together with the downstream endodermal enhancers (black ovals), the centrally conserved domain (CCD; DNase I hypersensitive sites, white box) (41) and the ICR. A matrix attachment region (MAR3; white box) and the differentially methylated regions 1 and 2 (DMR1 and DMR2; grey lollipops) are also depicted. The *Igf2* promoters (P0, P1, P2 and P3) are indicated by arrows, BamHI restriction sites by vertical lines and sites investigated in 3C assays by white arrows. The primer used as the anchor (close to BamHI site 0 and to the endodermal enhancers) is represented by a black arrow. (**B**) The graph represents the measured relative interaction frequencies between the endodermal enhancers (anchor/BamHI site 0) and each of the BamHI sites investigated as a function of the genomic distances (in bp). Data were collected from samples issued from 7-days-old (white circles) or 30-days-old (black diamonds) mouse livers. Parts of the graph that are included into the noise band or those that reflect the side effect are shadowed in grey. Error bars represent SEM of three independent 3C assays.

the interaction with DMR1 (Site 19) is abolished and that the enhancers are now interacting with the entire *Igf2* gene body (Sites 18–15) (Figure 2E, black squares). This suggests that, in this mutant, *Igf2* expression on the maternal allele, that results from loss of imprinting [(29) and Figure 6B], leads to a pattern of interactions that is clearly different from that observed on the wild-type paternal allele (i.e. the interactions are not restricted to *Igf2* DMRs). Interestingly, the loss of the paternal-specific enhancers/DMR1 interaction indicates that, in this context, the maternal H19Δ13 deletion induces a *trans*-effect on *Igf2*. Upon paternal inheritance of the H19Δ13 deletion (Figure 2E, grey triangles), the interactions with the DMR1, the DMR2 and the intergenic regions (Sites 19, 16, 12 and 10) are abolished. Interestingly, however, the endodermal enhancers are now exclusively interacting with the P1 promoter of the *Igf2* gene (Site 18) which is known as a liver-specific promoter (27,28,30), and *Igf2* expression (Supplementary Figure S1A) and imprinting (Figure 6B) are not significantly affected. We conclude that, on the paternal allele, the enhancers/*Igf2* DMRs interactions depend on an intact ICR/*H19* gene region.

The *Igf2*/*H19* intergenic region interacts with the enhancers, but not the *Igf2* DMRs

To better characterize the novel interaction between the enhancers and the *Igf2*/*H19* intergenic region, we performed 3C-qPCR experiments to analyse the interaction pattern between the intergenic region (Site 10, anchor) and the entire *Igf2*/*H19* locus (Figure 3A). We confirmed that, in the 7 days-old mouse liver, this region interacts with the endodermal enhancers (Site 0) (Figure 3B), but not, for example, with the cs9 (Site −6), a sequence that display mesodermic enhancer activity (31,32). The intergenic region displays significant contacts with the *Igf2* gene body and promoters but, interestingly, no interaction were found with the *Igf2* DMRs (Sites 19 and 16). This result indicates that the endodermal enhancers interacts with the intergenic region separately from their interactions with the *Igf2* DMRs.

Characterization of a novel imprinted non-coding RNA: the *PIHit*

Since the *H19* endodermal enhancers interact with an *Igf2*/*H19* intergenic region (BamHI site 10 is located ∼20.6 kb downstream to the *Igf2* gene) and that this interaction disappears when the *Igf2* and *H19* genes become repressed (Figure 1B), we hypothesized that this intergenic region might be transcribed in the 7-days-old mouse liver. Although no peculiar transcriptional activity was known in this intergenic region, we noticed that it is hosting several mouse 'LongSAGE tags' (see for example, chr7:142 430 105–142 430 125 on mouse Feb.2006/mm8 assembly). To assess transcription, we performed a northern blot experiment on total RNA extracted from livers at several post-natal stages. Hybridization with a probe located within the intergenic region (Figure 4A)

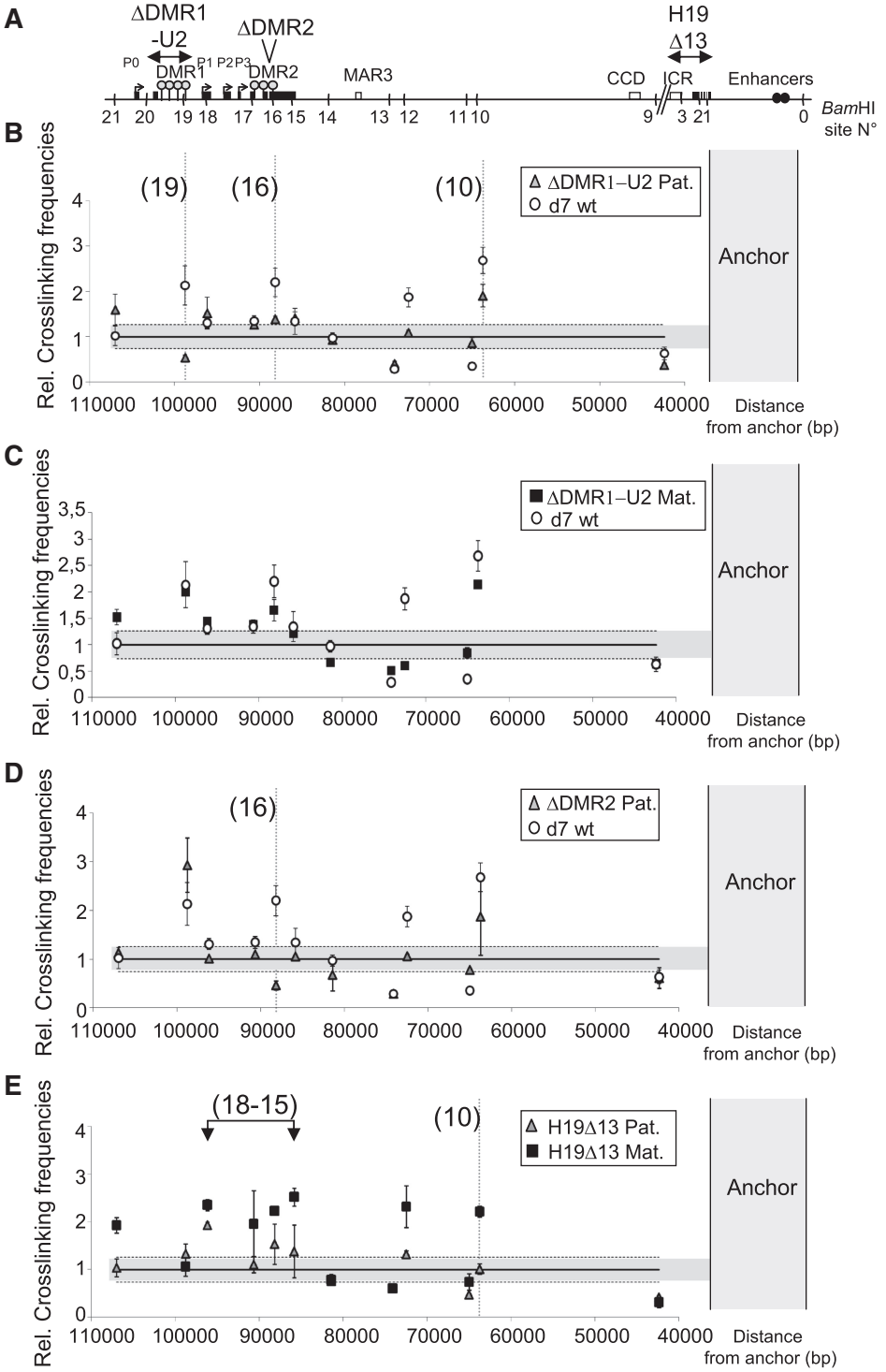

Figure 2. Interactions between endodermal enhancers and *Igf2* DMRs are paternal-chromosome specific. (**A**) Schematic representation of the mouse *Igf2*/*H19* locus showing the locations of the ΔDMR1-U2, ΔDMR2 and H19Δ13 deletions. The genomic elements depicted are as indicated in Figure 1A. (**B–D**) The graph represents the measured relative interaction frequencies between the endodermal enhancers (anchor/BamHI site 0) and each of the BamHI sites investigated as a function of the genomic distances (in bp). Data were collected from 7-days-old mouse liver samples issued from wild-type animals (white circles in panels B–D) or from mutant strains carrying either a paternal inheritance of the ΔDMR1-U2, ΔDMR2 or H19Δ13 deletions (grey triangles in panels B, D and **E**, respectively) or a maternal inheritance of the ΔDMR1-U2 or H19Δ13 deletions (black squares in panel C and E, respectively). The noise band is shadowed in grey. Error bars represent SEM of three independent 3C assays.

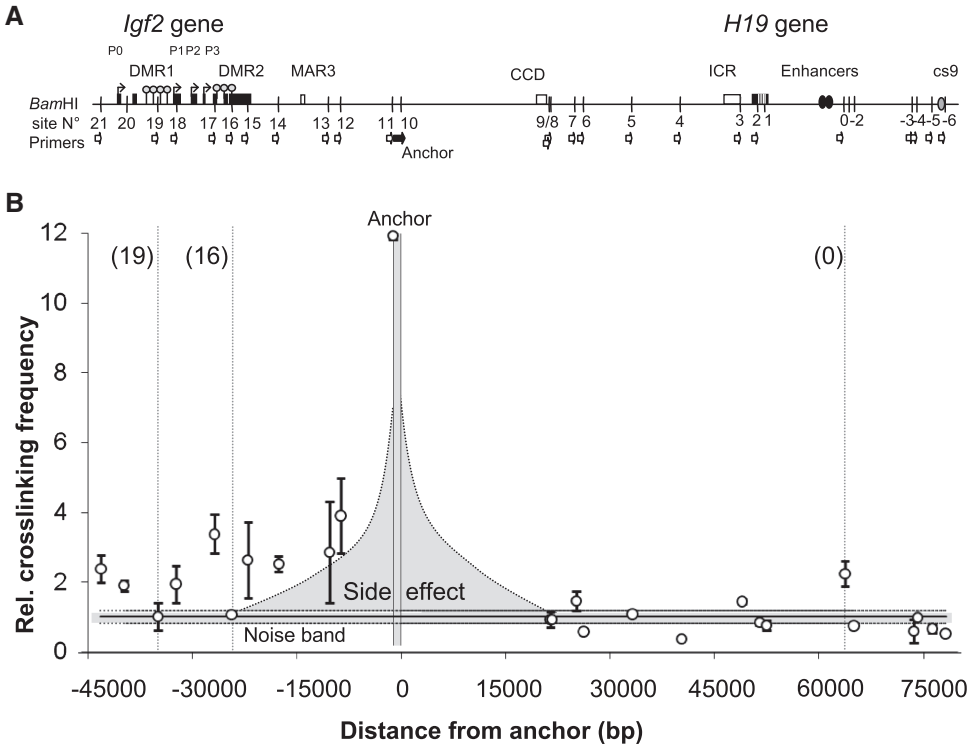

Figure 3. The intergenic *Igf2*/*H19* region interacts with the *Igf2* gene body but not the DMRs. (**A**) Schematic representation of the mouse *Igf2*/*H19* locus. The anchor (BamHI site 10) is indicated as a black arrow. The position of a mesodermic enhancer (cs9; grey oval) is also shown. The other genomic elements depicted are as indicated in Figure 1A. (**B**) The graph represents the measured relative interaction frequencies between the intergenic region (anchor/BamHI site 10) and each of the BamHI sites investigated as a function of the genomic distances (in bp). Data were collected from samples issued from 7-days-old wild-type mouse livers (white circles). Parts of the graph that are included into the noise band or those that reflect the side effect are shadowed in grey. Error bars represent SEM of two independent 3C assays.

reveals that transcriptional activity can be detected between post-natal Days 2 and 9 (Figure 4B, left panel). The region produces transcripts of heterogeneous sizes (ranging from 5 or 6 kb to 0.5 kb) that are detected as a smear in northern blot experiments. We subsequently hybridized the same northern blot membrane with an *Igf2*-specific probe located in *Igf2* exon 6 (Figure 4A). As expected, this probe revealed the intact 3.8 kb *Igf2* mRNAs (P1 and P3 transcripts) (Figure 4B, right panel), thus demonstrating the integrity of the RNA preparations used in this experiment. A northern blot on a preparation of polyadenylated RNAs showed that the intergenic transcripts are present in the unpolyadenylated fraction while, as expected, the *Igf2* mRNAs are retained into the polyadenylated fraction (Supplementary Figure S2).

To further investigate the expression pattern of this novel intergenic transcription, we then analysed the expression levels by RT–qPCR in the 7-days-old post-natal mouse liver at several intergenic positions (Figure 4C). No significant expression could be detected further upstream (towards the *Igf2* gene) at position −0.78 kb. Interestingly, we noticed that transcript levels are quite similar throughout 6 kb but decrease dramatically further downstream to reach very low amounts at positions ∼15 kb (Figure 4C). These results agree with northern blot experiments showing that most transcripts produced from this intergenic region are smaller than 5–6 kb (Figure 4B).

As suggested by northern blotting (Figure 4B), transcript levels, that are moderate in the neonate, increase suddenly 8 days after birth (Figure 4D) to reach levels about three times higher than *Gapdh* mRNA levels. This expression then decreases rapidly and full repression occurs during the third post-natal week (Figure 4D). This pattern of expression is similar at three distinct intergenic locations where it was assayed (+0.26, +11.1, +14.4 kb) (Figure 4D).

We then performed RT–qPCR on total RNA prepared from several mouse tissues. Expression was first checked at site 11 (with PCR primers located 0.06 kb upstream and 0.16 kb downstream of this site). RNA levels were relatively high in the post-natal d7 liver (∼36 times less than *Igf2* mRNA levels), much weaker in the newborn kidney, tongue and brain (∼400 time less expressed than *Gapdh* and *Igf2* mRNA levels) and very weak (about 2500 time less than *Gapdh* and *Igf2* mRNA levels) in the heart (Figure 5A).

Using a forward PCR primer located at position +0.26 kb (relative to Site 11) and a reverse primer +3.6 kb downstream (Figure 4A), we were able to PCR amplify a cDNA as a single amplicon of the expected size (3.34 kb), showing that no significant RNA processing occurs for transcripts produced from that region (data not shown). We then assessed the transcriptional orientation of these RNAs at three distinct sites along the

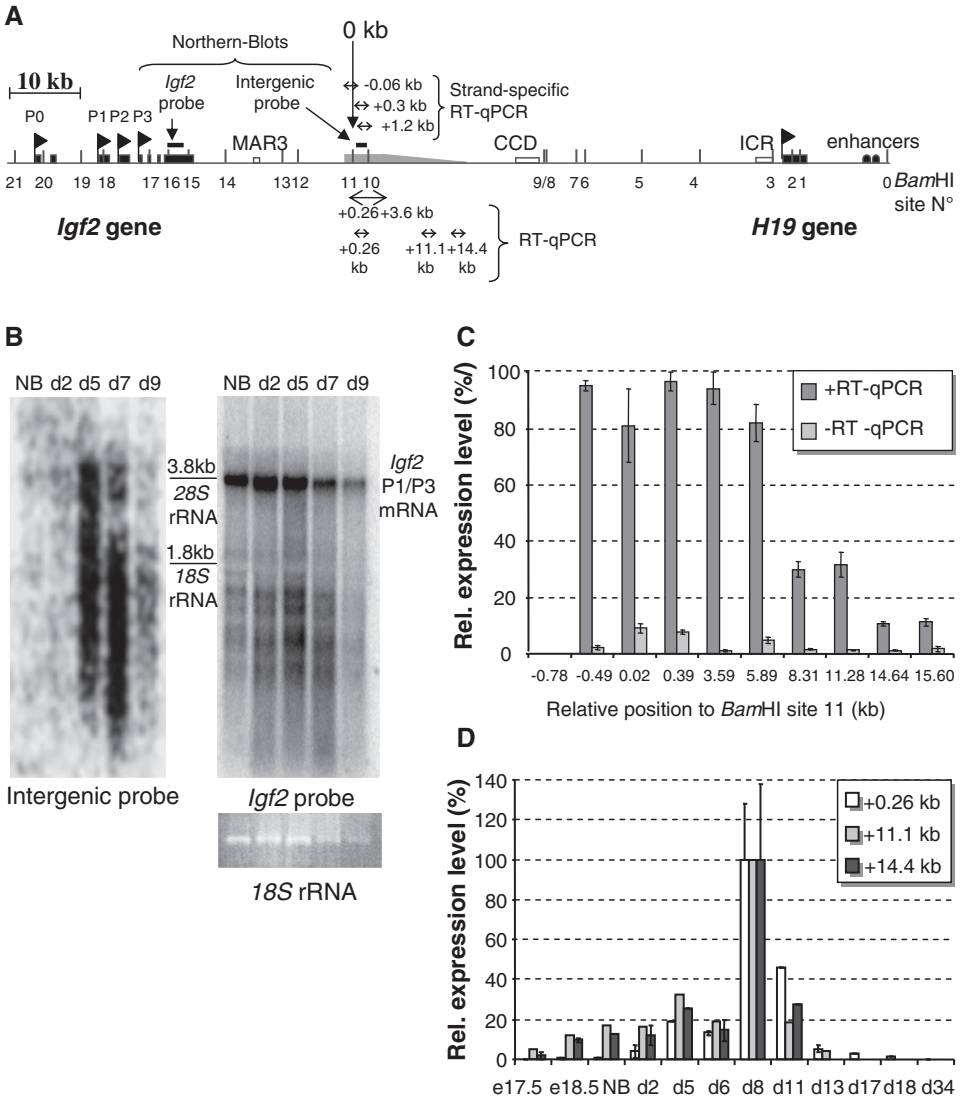

Figure 4. The *Igf2*/*H19* intergenic region that interacts with the endodermal enhancers is transcribed. (**A**) Schematic representation of the *Igf2*/*H19* locus showing the location of the northern blot probes and RT–PCR primers used to characterize the intergenic transcripts. The transcribed intergenic region is depicted in grey and several genomic elements are also indicated. Except opposite statement, all positions given in the Result section or in the figure are intended relative to BamHI site 11, located at chr7: 149.817.140 on mouse July 2007/mm9 assembly. (**B**) Northern blots showing the expression patterns of the intergenic region (left panel) or the *Igf2* mRNAs (right panel). Total RNAs were prepared from newborn (NB) livers or from post-natal (d2, d5, d7 and d9) mouse livers and analysed by Ethidium bromide staining of the agarose/formaldehyde gel (lower panel on the right) before being transferred to a nylon membrane and hybridized by an intergenic probe (left panel). As a quality control of RNA preparations, the same membrane was subsequently re-hybridized with an *Igf2* probe (upper panel on the right). The position of the *Igf2* P1 and P3 mRNA transcripts (the P2 transcript has very low expression levels in liver) and of the 28S and 18S rRNA (3.8 and 1.8 kb, respectively) are indicated. (**C**) The relative expression levels of intergenic transcripts (black bars) were determined by RT–qPCR at increasing genomic positions as indicated on the figure. Control reactions with no reverse transcription (−RT) have also being quantified (grey bars). Data was quantified relative to *Gapdh* mRNA levels and normalized to the higher RNA level quantified in the series. Liver sample is from d7 mice; the other samples were prepared from newborn mice. (**D**) Intergenic transcripts were quantified by RT–qPCR at three distinct genomic positions (+0.26, +11.1 and +14.4 kb) in mouse liver samples at the following developmental stages: embryos 17.5 and 18.5 *dpc* (e17.5 and e18.5), newborn (NB), post-natal Day 2, 5, 6, 8, 11, 13, 17, 18, 34 (d2–d34). In panels B and C, error bars represent s.e.m. of quantifications performed on two independent RT reactions. Data were normalized as described above. RT–qPCR primer sequences are given in the Supplementary Table S2.

intergenic region (−0.06, +0.3, +1.2 kb) by using strand-specific reverse transcription and qPCR amplifications (ssRT–qPCR). This showed that transcription occurs in the same ('sense') orientation as the *Igf2* and *H19* genes (Table 1). Finally, we showed that the proportion of these transcripts in nuclear RNA preparations is relatively low when compared to a typical nuclear RNA (*U3* snoRNA),

Table 1. Transcriptional orientation

Position (kb)[a]	−0.06	+0.3	+1.2
Sense-specific RT primer (%)	98.8	91.7	100
Antisense-specific RT primer (%)	1.1	8.2	0

[a]Relative to BamHI site 11.

but it is much higher than a classical messenger RNA (*Igf2* mRNA) (Supplementary Figure S3).

Although the intergenic transcripts appear as a smear on northern blots, the fact that their expression pattern is identical throughout ~15 kb (Figure 4D) raised the possibility that they could originate from a single transcriptional start site (TSS). To identify this TSS, we were helped by genomic HRS assays (25) showing that the most 5′ transcribed region (Figure 4C) corresponds precisely to a 'HRS1' for which retention into the nuclear matrix fraction exclusively occurs on the paternal allele and correlates with transcription (Supplementary Figure S4). We thus designed 5′-RACE primers located into the 686 bp StyI restriction fragment corresponding to this HRS1 (see Supplementary Figure S4B) and successfully amplified a single band from the capped fraction of d7 mouse liver RNAs (Supplementary Figure S5A). Sequencing of this PCR product then allowed us to map the cap site 535 bp upstream of Site 11 (Supplementary Figure S5B). We conclude that the intergenic transcripts are capped and initiated from a single TSS (TSS at position: chr7: 149 816 606 on mouse July 2007/mm9 assembly).

Since the HRS1, containing the TSS, was retained in HRS assays only on the paternal allele (Supplementary Figure S4C), we postulated that this novel transcript may be imprinted. We thus prepared total RNA from livers of 7-days-old hybrid mice (issued from *M. m. domesticus* female X *SDP711* male or the reverse cross), and performed allele-specific RT–qPCR, at three distinct sites along the intergenic region (−0.07 kb/+5.2 kb/+8.2 kb). These experiments showed that transcription occurs exclusively on the paternal chromosome (Figure 6A). Although expression levels are very low in most other tissues (Figure 5A), imprinted expression was also evidenced in the kidney, the heart, the tongue and the brain (Figure 5B). Finally, analysis of the transcribed region (UCSC server) shows that it displays a much higher sequence conservation index than surrounding sequences (Figure 7A). However, it contains only very short open reading frames that are not conserved in mammals (data not shown). We conclude that the intergenic transcriptional activity identified in this work produces a novel non-coding transcript which is paternally expressed/maternally imprinted, and we thus named it *PIHit*: Paternally-expressed *Igf2*/*H19* intergenic transcript.

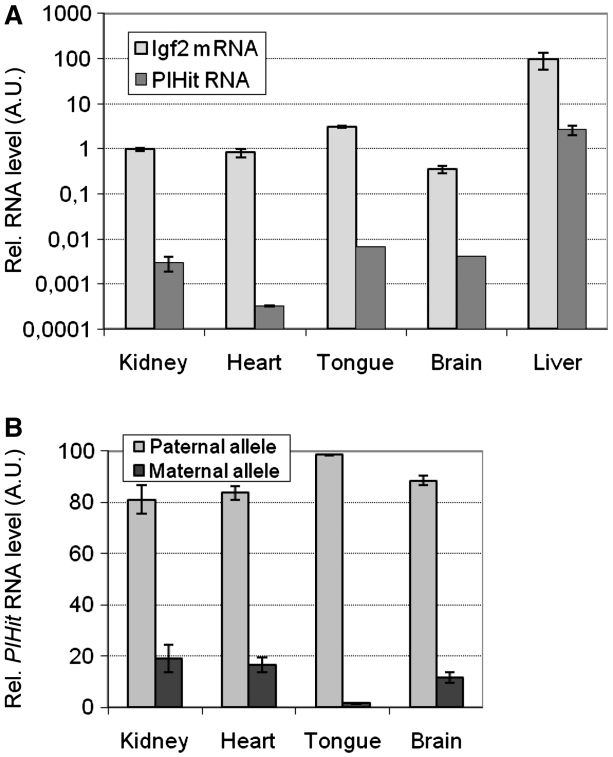

Figure 5. Analysis of intergenic transcription in several mouse tissues. (**A**) The relative expression levels of the *PIHit* (dark grey bars) or *Igf2* (light grey bars) RNAs were measured by RT–qPCR in samples issued from newborn (kidney, heart, tongue and brain) or post-natal d7 (liver) hybrid mice (issued from a cross between *SD7* females and *M. musculus domesticus* males). Data are normalized relative to *Gapdh* mRNA levels. (**B**) Allelic expression levels of the *PIHit* RNA were determined by allele-specific RT-qPCR in the above mentioned samples. Error bars represent SEM of quantifications performed on two independent RT reactions.

PIHit imprinting does not require an intact *ICR*/*H19* gene region

Since imprinting at the *Igf2*/*H19* locus depends on the ICR, we wanted to check whether the paternal chromosome-specific expression of *PIHit* is also controlled by this element. Upon paternal inheritance of the H19Δ13 deletion, that removes both the ICR and the *H19* gene, both *Igf2* [(29) and Figure 6B)] and *PIHit* (Figure 6C) remain imprinted and preferentially expressed from the paternal chromosome. However, we note that *PIHit* expression is dramatically reduced (Supplementary Figure S1B), suggesting that *PIHit* expression requires a paternal-specific feature (linked to the ICR/*H19* gene region) that favour its expression on this allele. This agrees with our finding that the interaction between the endodermal enhancers and the *PIHit* promoter region (site 10) depends on an intact ICR/*H19* gene region (Figure 2E). Furthermore, high paternal-specific expression of *PIHit* RNA on the paternal allele also requires an intact DMR1, but not DMR2, sequence (Supplementary Figure S1). Most surprisingly, while maternal inheritance of the H19Δ13 deletion leads, as expected (29), to the complete loss of *Igf2* imprinting (Figure 6B), it does not significantly affect *PIHit* imprinting (Figure 6C). This unexpected finding shows that the ICR/*H19* region is not required for proper imprinting of the *PIHit* locus.

Mapping of a discrete DMR at the *PIHit* locus

Genomic HRS assays had identified two HRS (HRS1 and HRS2) at the *PIHit* locus (Supplementary Figure S4). As seen previously, the HRS1 corresponds to the *PIHit* promoter region. Interestingly, HRS2 contains a G/C-rich sequence which is highly conserved among 30 mammalian species (Figure 7A). *PIHit* promoter displays a lower G/C content and the only other G/C-rich region identified at the *PIHit* locus (CpG1) is located at the

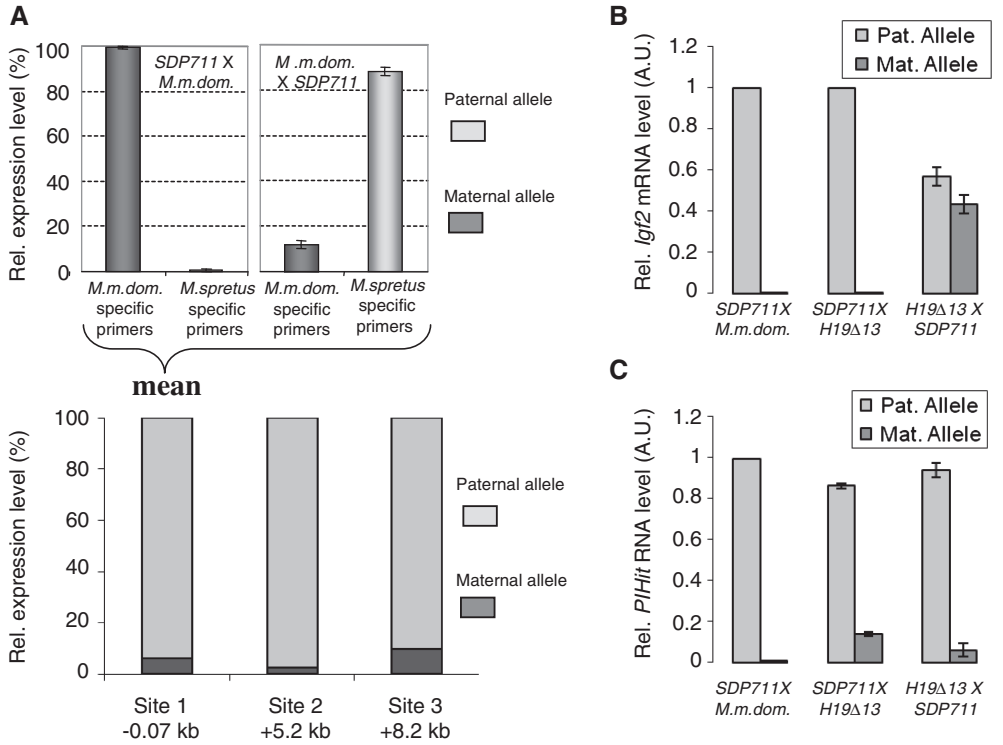

Figure 6. The *PIHit* RNA is a novel imprinted non-coding RNA. (**A**) The relative allelic expression levels were quantified by allele-specific RT-qPCR on total RNA from liver of hybrid mice issued from a cross between *M. musculus domesticus* (C57BL6/CBA F1) females and SDP711 males (upper right panel) or the reverse cross (*SDP711* female X *M. m. domesticus* males) (upper left panel). *SDP711* is a congenic mouse strain where the distal part of chromosome 7 and the proximal part of chromosome 11 are of *Mus spretus* origin. Data were normalized relative to *Gapdh* mRNA levels. Error bars represent SEM of quantifications performed on two independent RT reactions. The experiment was repeated at three distinct genomic sites (−0.07, +5.2 and +8.2 kb). All the data were combined by calculating the mean expression levels of each allele in both crosses to be finally presented into a single graph (lower panel). The relative allelic expression levels of the *Igf2* mRNA (**B**) or *PIHit* (**C**) were determined by allele-specific RT–qPCR on hybrid mice with paternal or maternal inheritance of the H19Δ13 deletion. Error bars represent SEM of quantifications performed on two independent RT reactions. Sequences of primers used in allele-specific RT–qPCR experiments are given in the Supplementary Table S8.

most 3′ part of the locus. Since DMRs are known in most imprinted genes, we hypothesized that the HRS2 and/or the CpG1 may correspond to such regions of allele-specific DNA methylation. We thus performed bisulphite sequencing experiments and showed that, remarkably, the most conserved sequence within the HRS2 displays a discrete but significant difference in the levels of DNA methylation between the two parental alleles ($P = 0.0233$; $n = 54$; Mann–Whitney U-test) (Figure 7B). Interestingly, in contrast to the methylation patterns observed in the liver for the *Igf2* DMRs (6,28), this *PIHit* DMR is more methylated on the maternal allele than on the paternal allele. Surrounding sequences did not reveal any significant allelic differences in DNA methylation levels. Finally, similar experiments performed at the CpG1 demonstrated that this region is quite heavily methylated on both alleles (data not shown). We conclude that the short 234 bp conserved sequence (chr7: 149 812 622–149 812 856 on mouse July 2007/mm9 assembly) located within the HRS2 corresponds to a discrete DMR (*PIHit* DMR). Since this *PIHit* DMR was quite narrow and discrete, we postulated that it may simply result from *PIHit* expression. To assess this hypothesis, we digested the *PIHit* DMR by the BceAI methylation-sensitive enzyme and thus measured the allelic methylation levels of the *PIHit* DMR in the mouse liver at different neonatal and post-natal stages. Again, a discrete but significant preferential maternal methylation was evidenced in all assayed samples (Figure 7C), including in the embryonic and neonatal livers at a time preceding the burst of *PIHit* expression (Figure 4). We conclude that the *PIHit* DMR is not just a mere consequence of *PIHit* expression.

DISCUSSION

In this work, using the 3C-qPCR assay (20), we investigated long-range chromatin interactions at the mouse *Igf2/H19* locus. These investigations lead us to discover a novel maternally imprinted region that produces, on the paternal chromosome, a liver-specific capped, but unpolyadenylated transcript, that we named the *PIHit* (paternally expressed *Igf2/H19* intergenic transcript). This transcript is a long heterogeneously sized RNA that can thus be considered as a novel imprinted macro non-coding RNA (33).

Since *PIHit* RNA is exclusively expressed from the paternal chromosome, we can reasonably assume that

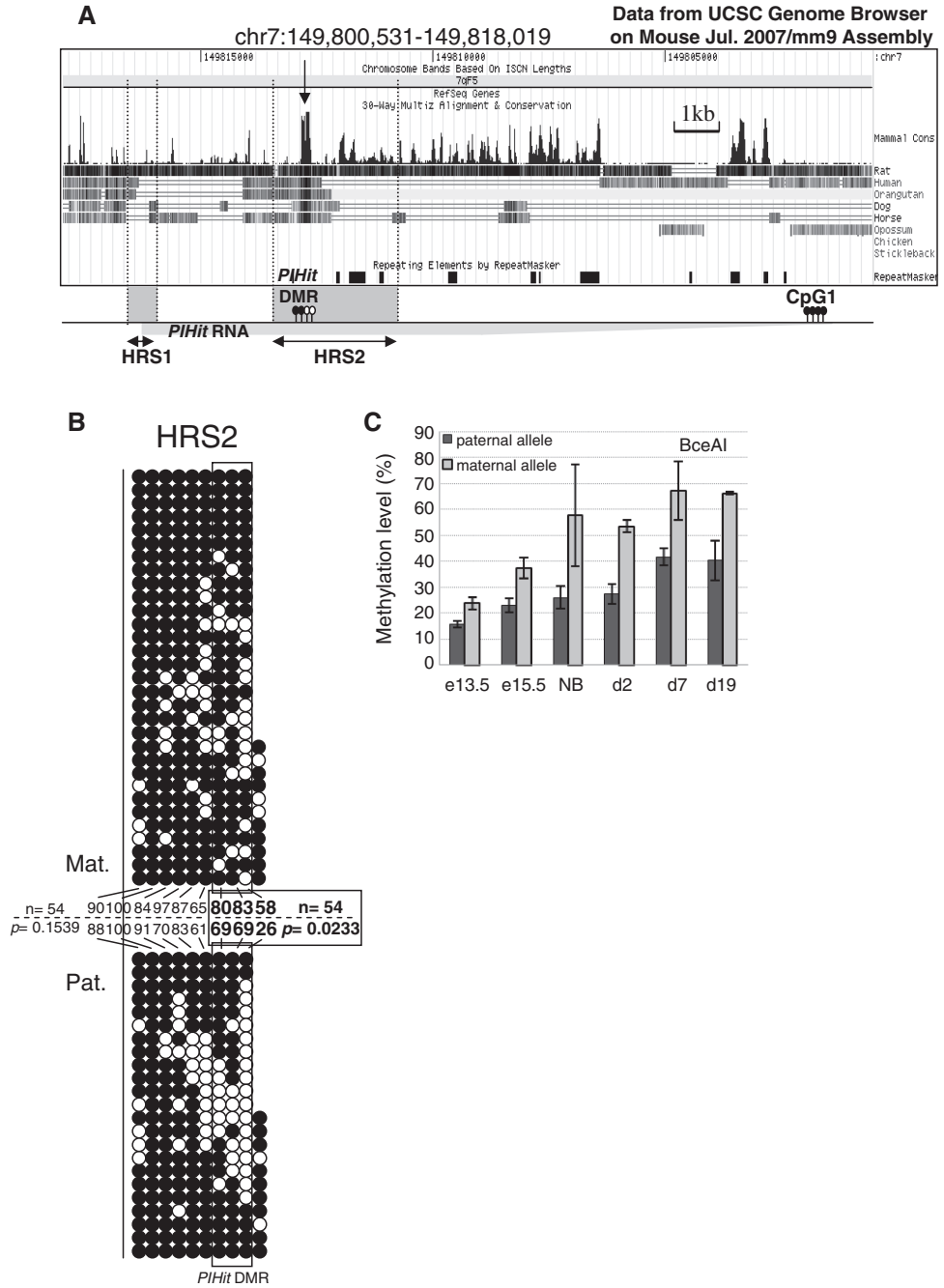

Figure 7. Mapping of a discrete differentially methylated region at *PIHit* locus. (**A**) The figure displays the *PIHit* locus into a UCSC Genome Browser window obtained on the mouse July 2007/mm9 assembly (chr7:149 800 531–149 818 019). It shows the sequence conservation index ('Mammal Cons.' lane) and the location of repeats (black boxes; 'RepeatMasker' lane). One can note that the HRS2 contains a sequence (chr7:149 812 622–149 812 856) that is highly conserved in mammals (black vertical arrow). The positions of the *PIHit* DMR (see below) and of a CpG-rich sequence (CpG1) are indicated below the UCSC window. The transcribed region is depicted in grey. (**B**) The methylation pattern of the HRS2 sequence was determined in the 7-days-old mouse liver by bisulphite sequencing. The mean methylation levels (%) of each CpG of the *PIHit* DMR are indicated on the figure. A discrete differentially methylated region (*PIHit* DMR), containing only three CpG and corresponding to a sequence highly conserved in mammals (see above), is significantly more methylated on the maternal than on the paternal chromosome ($P = 0.0233$; $n = 54$; Mann–Whitney U-test). No significant difference was found outside this region ($P = 0.1539$; $n = 54$; Mann–Whitney U-test). (**C**) Allelic methylation levels of the *PIHit* DMR were estimated in the mouse liver, at the indicated developmental stages (NB: newborn), by digestion of the genomic DNA with the methylation-sensitive BceAI restriction enzyme and quantifications by allele-specific qPCR. Noteworthy, this BceAI site encompasses the CpG dinucleotide that displayed the strongest difference of allelic methylation in the bisulphite experiment (58/26%) (Figure 7B). Error bars represent SEM of quantifications performed on at least two independent BceAI digestions.

the interaction between the enhancers and the *PIHit* locus occurs on this chromosome. HRS data strengthen this view since both the HRS1 and HRS2 are retained on paternal allele (Supplementary Figure S4). This situation is reminiscent of the observations made for the DMR2 sequence where the paternal-specific interaction with the endodermal enhancers (Figure 2D) correlates with retention into the nuclear matrix (25).

In d7 liver, the *Igf2* gene is mainly expressed from promoter P3 while expression from promoter P2 and from the liver-specific promoter P1 is much lower (27,28). Our results clearly show that the interactions of the endodermal enhancers with the *Igf2* gene occur preferentially with the *Igf2* DMRs rather than with the promoters (Figure 1B) and that these interactions take place exclusively on the paternal chromosome (Figure 2B and D).

Our results also indicate that, in the liver, the activity of the DMR2 that augments *Igf2* transcription (8) may involve the recruitment of the endodermal enhancers. Furthermore, since the endodermal enhancers do not significantly interact with the *Igf2* promoters, one can think that, on that chromosome, the endodermal enhancers may not act at the transcriptional initiation step but rather at a later stage-like, for example, transcriptional elongation or termination. Our results also demonstrate that the interaction of the endodermal enhancers with the DMR2 requires the presence of both the DMR1 and the ICR/*H19* gene regions in *cis* while the interaction with the DMR1 depends on an intact ICR/*H19* gene region but not on the DMR2 sequence (Figure 2). These observations are in perfect agreement with the hierarchy that was previously proposed for DMRs at the *Igf2* locus (34). Interestingly, we found that the endodermal enhancers interact with the *PIHit* locus separately from their interactions with the *Igf2* DMRs (Figure 3B). This suggests that the two types of interactions may be hampering each other. Globally, these results lead us to propose a novel model for chromatin folding at the *Igf2*/*H19* locus on the paternal chromosome whereby the recruitment of the *PIHit* locus into a chromatin hub involving the enhancers and *Igf2* DMRs acts as a decoy for such interactions, thus contributing to fine tuning of *Igf2* expression (Figure 8). A recent work at the human *IGF2*/*H19* locus shows that chromatin folding on the paternal chromosome is mediated through a network of CTCF/Cohesin contacts (18). Interestingly, chromatin folding as presented in our model is fully compatible with these findings. Indeed, in the human, CTCF binds to three regions on the paternal *IGF2*/*H19* chromosome: the first (CTCF AD) is located upstream the *Igf2* gene, the second is the centrally conserved DNase I hypersensitive domain (CCD) and the last (CTCF DS) maps downstream to the *H19* enhancers (18). Interestingly, all three regions are implicitly found in close vicinity in our model (Figure 8). However, it remains to be shown whether these regions also bind CTCF in the mouse.

This model suggests that *PIHit* transcription may be required to counteract a mechanism that favours high-*Igf2* expression levels in the post-natal liver (8). However, an unforeseen obstacle prevented us from performing RNA interference experiments to investigate *PIHit* functions. Indeed, high-*PIHit* expression levels were found only in the post-natal mouse liver (Figures 4 and 5) and, despite intensive efforts, we were unable to find any cultured cell lines expressing significant *PIHit* RNA levels. Finally, none of the targeted deletions available at the *Igf2*/*H19* locus (35) involve the *PIHit* region and therefore, in the present 'state of the art', *PIHit* function could only be experimentally addressed by performing a novel targeted deletion at this locus.

Globally, our results agree with previous data indicating that, on the paternal allele, the enhancers interact with the *Igf2* gene region (18), upstream of the ICR (11). However, published results differ in suggesting that they interact either with the *Igf2* promoters (13,19) or with the entire gene body (11). Our work shows that, in post-natal Day 7 mouse liver, the enhancers interact with the *Igf2* DMRs but not significantly with the *Igf2* promoters. The difference with published results showing specific interactions with the *Igf2* promoters may simply arise from the nature of the samples analysed. Indeed, previous studies focused on the foetal (12) or neonatal (11,19,36) liver. In these tissues, *Igf2* expression levels are at least 2.5–3 times lower than in the 7-days-old mouse liver (27,28) where the endodermal enhancers are known to have a strong effect to augment *Igf2* expression (37). Furthermore, *PIHit* expression is also very low in the neonatal liver (Figure 4). Finally, only the most recent studies performed at the human *IGF2*/*H19* locus (13,18) have used quantitative 3C assays, which is of precious help to fully discriminate between functional interactions and random collision events (38). However, again, these latter experiments where performed in cells that expresses low levels of *IGF2* mRNA.

Noticeably, although the maternal *Igf2* allele is re-expressed upon maternal transmission of the H19Δ13 deletion (29) (Figure 6B), our experiments show that this re-expression occurs in a context of high-order chromatin folding (Figure 2E), which is somewhat different from that of the wild-type paternal allele (Figure 1B). This can be explained by the size of the deletion, that removes 13 kb of genomic sequence, as well as by the fact that this deletion results in very low levels of the *H19* RNA (29), which is known to act as a *trans*-riboregulator that represses *Igf2* expression (1). Actually, *trans*-effects of *H19* deletions on *Igf2* have been known for a long time. For example, *H19* maternal deletion is known to decrease significantly methylation levels of the *Igf2* DMR2 on the paternal allele (39). These *trans*-effects may also explain another intriguing observation. Indeed, upon maternal transmission of the H19Δ13 deletion the interaction of the enhancers with the DMR1 is abolished (site 19 in Figure 2E). Since this interaction takes place on the paternal allele and this allele is intact in these mice, this means that the maternal deletion has a *trans*-effect on that interaction. Finally, upon maternal transmission of the H19Δ13 deletion, the enhancers interact with the entire *Igf2* gene body, including the *Igf2* promoters (Figure 2E). Therefore, it is possible that, in that specific case, the enhancers track along the *Igf2* gene until they find a suitable

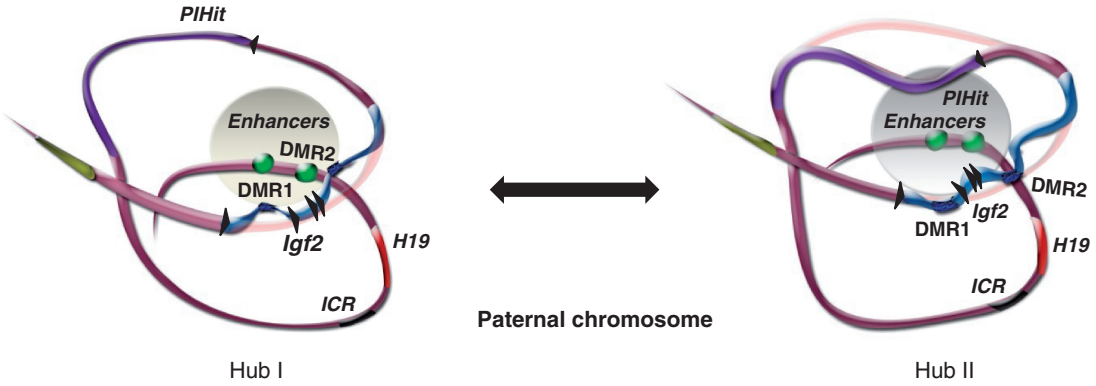

Figure 8. Model for tri-dimensional folding of the mouse *Igf2*/*H19* locus on the paternal allele. This model is based on the 3C-qPCR data obtained in the 7-days-old mouse liver (Figures 1–3). On the paternal chromosome, the endodermal enhancers, located downstream the *H19* gene, interact either with the *Igf2* DMRs or with the *PIHit* locus. These two types of interactions appear to be exclusive, suggesting that they are hampering each other. Therefore, we propose that two alternative chromatin hubs (grey ovals) may occur at this locus on the paternal chromosome. In the first one, the enhancers would interact with the methylated *Igf2* DMRs leading to high *Igf2* gene expression. A second type of chromatin hub would form when the *PIHit* locus is entering the hub to interact with the enhancers resulting in *PIHit* RNA expression and exclusion of the *Igf2* DMR, thus contributing to fine tuning of *Igf2* expression. These distinct chromatin hubs may form either stably, via chromatin loops, in two separate liver cell populations or they may occur in a more dynamic way through transient but specific interactions that take place in the whole cell population analysed. Note that, according to this model, both ends of the *Igf2*/*H19* locus and a region downstream of the *PIHit* sequence are found in close spatial vicinity. Interestingly, in the human, chromatin folding on the paternal chromosome is mediated through a network of CTCF/Cohesin contacts that involves these three regions (18).

promoter to interact with and thus in this context, our data are compatible with an enhancer tracking model (19,40).

One surprising finding is that, while an intact ICR/*H19* region is required on the paternal allele to maintain high *PIHit* expression levels (Supplementary Figure S1), it is dispensable for *PIHit* repression on the maternal allele (Figure 6C). We can, therefore, formulate two hypotheses to explain *PIHit* imprinting: either repression is the default state of the *PIHit* locus, and monoallelic expression of *PIHit* then results from the combined paternal-specific activities of the ICR/*H19* and *Igf2* DMR1 regions that both favour *PIHit* expression (Supplementary Figure S1), or a yet unknown Imprinting Control Region is required on the maternal chromosome to mediate *PIHit* repression. Since this locus has been extensively investigated and that many deletions have been generated in the mouse (35), it seems unlikely that a primary imprinting centre would have escaped the wealth of recent investigations. However, one remaining possibility may be that the discrete *PIHit* DMR that we have identified in this work is involved in the establishment and/or the maintenance of *PIHit* imprinting on the maternal allele. Interestingly, preferential methylation on the maternal chromosome precedes *PIHit* expression and therefore does not appear to simply result from monoallelic expression of this locus (Figure 7C). Inactivation of this sequence in the mouse will therefore also be required to clarify this point.

SUPPLEMENTARY DATA

Supplementary Data are available at NAR Online.

ACKNOWLEDGEMENTS

The authors are grateful to W. Reik for providing the ΔDMR1-U2 and ΔDMR2 mouse strains and to S. Tilghman for the H19Δ13 mice. The authors thank Luisa Dandolo, Robert Feil, Laurent Journot, Julie Borgel and Sylvain Guibert for stimulating scientific discussions and the staff from the animal unit at the Institut de Génétique Moléculaire for technical assistance.

FUNDING

Association pour la Recherche contre le Cancer (ARC); Centre National de la Recherche Scientifique (PIR Interface 106245); Agence Nationale de la Recherche (ANR-07-BLAN-0052-02 to T.F.); CEFIC-Long-Range Research Initiative (LRI-EMSG49-CNRS-08 to M.W.); Ligue Nationale Contre le Cancer (Ardèche section) (to F.C.). Funding for open access charge: Centre National de la Recherche Scientifique (C.N.R.S.), France.

Conflict of interest statement. None declared.

REFERENCES

1. Gabory,A., Ripoche,M.A., Le Digarcher,A., Watrin,F., Ziyyat,A., Forné,T., Jammes,H., Ainscough,J.F., Surani,M.A., Journot,L. *et al*. (2009) *H19* acts as a trans regulator of the imprinted gene network controlling growth in mice. *Development*, **136**, 3413–3421.
2. Varrault,A., Gueydan,C., Delalbre,A., Bellmann,A., Houssami,S., Aknin,C., Severac,D., Chotard,L., Kahli,M., Le Digarcher,A. *et al*. (2006) *Zac1* regulates an imprinted gene network critically involved in the control of embryonic growth. *Dev. Cell.*, **11**, 711–722.

3. Szabo,P., Tang,S.H., Rentsendorj,A., Pfeifer,G.P. and Mann,J.R. (2000) Maternal-specific footprints at putative CTCF sites in the *H19* imprinting control region give evidence for insulator function. *Curr. Biol.*, **10**, 607–610.
4. Bell,A.C. and Felsenfeld,G. (2000) Methylation of a CTCF-dependent boundary controls imprinted expression of the *Igf2* gene. *Nature*, **405**, 482–485.
5. Hark,A.T., Schoenherr,C.J., Katz,D.J., Ingram,R.S., Levorse,J.M. and Tilghman,S.M. (2000) CTCF mediates methylation-sensitive enhancer-blocking activity at the *H19*/*Igf2* locus. *Nature*, **405**, 486–489.
6. Feil,R., Walter,J., Allen,N.D. and Reik,W. (1994) Developmental control of allelic methylation in the imprinted mouse *Igf2* and *H19* genes. *Development*, **120**, 2933–2943.
7. Constancia,M., Dean,W., Lopes,S., Moore,T., Kelsey,G. and Reik,W. (2000) Deletion of a silencer element in *Igf2* results in loss of imprinting independent of *H19*. *Nat. Genet.*, **26**, 203–206.
8. Murrell,A., Heeson,S., Bowden,L., Constancia,M., Dean,W., Kelsey,G. and Reik,W. (2001) An intragenic methylated region in the imprinted *Igf2* gene augments transcription. *EMBO Rep.*, **2**, 1101–1106.
9. Phillips,J.E. and Corces,V.G. (2009) CTCF: master weaver of the genome. *Cell*, **137**, 1194–1211.
10. Murrell,A., Heeson,S. and Reik,W. (2004) Interaction between differentially methylated regions partitions the imprinted genes *Igf2* and *H19* into parent-specific chromatin loops. *Nat. Genet.*, **36**, 889–893.
11. Kurukuti,S., Tiwari,V.K., Tavoosidana,G., Pugacheva,E., Murrell,A., Zhao,Z., Lobanenkov,V., Reik,W. and Ohlsson,R. (2006) CTCF binding at the *H19* imprinting control region mediates maternally inherited higher-order chromatin conformation to restrict enhancer access to *Igf2*. *Proc. Natl Acad. Sci. USA*, **103**, 10684–10689.
12. Yoon,Y.S., Jeong,S., Rong,Q., Park,K.Y., Chung,J.H. and Pfeifer,K. (2007) Analysis of the *H19*ICR insulator. *Mol. Cell Biol.*, **27**, 3499–3510.
13. Nativio,R., Wendt,K.S., Ito,Y., Huddleston,J.E., Uribe-Lewis,S., Woodfine,K., Krueger,C., Reik,W., Peters,J.M. and Murrell,A. (2009) Cohesin is required for higher-order chromatin conformation at the imprinted *IGF2-H19* locus. *PLoS Genet.*, **5**, e1000739.
14. Parelho,V., Hadjur,S., Spivakov,M., Leleu,M., Sauer,S., Gregson,H.C., Jarmuz,A., Canzonetta,C., Webster,Z., Nesterova,T. *et al.* (2008) Cohesins functionally associate with CTCF on mammalian chromosome arms. *Cell*, **132**, 422–433.
15. Rubio,E.D., Reiss,D.J., Welcsh,P.L., Disteche,C.M., Filippova,G.N., Baliga,N.S., Aebersold,R., Ranish,J.A. and Krumm,A. (2008) CTCF physically links cohesin to chromatin. *Proc. Natl Acad. Sci. USA*, **105**, 8309–8314.
16. Stedman,W., Kang,H., Lin,S., Kissil,J.L., Bartolomei,M.S. and Lieberman,P.M. (2008) Cohesins localize with CTCF at the KSHV latency control region and at cellular *c-myc* and *H19*/*Igf2* insulators. *EMBO J.*, **27**, 654–666.
17. Wendt,K.S., Yoshida,K., Itoh,T., Bando,M., Koch,B., Schirghuber,E., Tsutsumi,S., Nagae,G., Ishihara,K., Mishiro,T. *et al.* (2008) Cohesin mediates transcriptional insulation by CCCT C-binding factor. *Nature*, **451**, 796–801.
18. Nativio,R., Sparago,A., Ito,Y., Weksberg,R., Riccio,A. and Murrell,A. (2011) Disruption of genomic neighbourhood at the imprinted *IGF2-H19* locus in Beckwith-Wiedemann syndrome and Silver-Russell syndrome. *Hum. Mol. Genet.*, **20**, 1363–1374.
19. Engel,N., Raval,A.K., Thorvaldsen,J.L. and Bartolomei,S.M. (2008) Three-dimensional conformation at the *H19*/*Igf2* locus supports a model of enhancer tracking. *Hum. Mol. Genet.*, **17**, 3021–3029.
20. Hagège,H., Klous,P., Braem,C., Splinter,E., Dekker,J., Cathala,G., de Laat,W. and Forné,T. (2007) Quantitative analysis of chromosome conformation capture assays (3C-qPCR). *Nat. Protoc.*, **2**, 1722–1733.
21. Sasaki,H., Jones,P.A., Chaillet,J.R., Ferguson-Smith,A.C., Barton,S.C., Reik,W. and Surani,M.A. (1992) Parental imprinting: potentially active chromatin of the repressed maternal allele of the mouse *insulin-like growth factor II* (*Igf2*) gene. *Genes Dev.*, **6**, 1843–1856.
22. Braem,C., Recolin,B., Rancourt,R.C., Angiolini,C., Barthes,P., Branchu,P., Court,F., Cathala,G., Ferguson-Smith,A.C. and Forné,T. (2008) Genomic matrix attachment region and chromosome conformation capture quantitative real time PCR assays identify novel putative regulatory elements at the imprinted *Dlk1*/*Gtl2* locus. *J. Biol. Chem.*, **283**, 18612–18620.
23. Lutfalla,G. and Uzé,G. (2006) Performing quantitative reverse-transcribed polymerase chain reaction experiments. *Methods Enzymol.*, **410**, 386–400.
24. Milligan,L., Antoine,E., Bisbal,C., Weber,M., Brunel,C., Forné,T. and Cathala,G. (2000) *H19* gene expression is up-regulated exclusively by stabilization of the RNA during muscle cell differentiation. *Oncogene*, **19**, 5810–5816.
25. Weber,M., Hagège,H., Murrell,A., Brunel,C., Reik,W., Cathala,G. and Forné,T. (2003) Genomic imprinting controls matrix attachment regions in the *Igf2* gene. *Mol. Cell Biol.*, **23**, 8953–8959.
26. Weber,M., Hagège,H., Lutfalla,G., Dandolo,L., Brunel,C., Cathala,G. and Forné,T. (2003) A real-time polymerase chain reaction assay for quantification of allele ratios and correction of amplification bias. *Anal. Biochem.*, **320**, 252–258.
27. Hagège,H., Nasser,R., Weber,M., Milligan,L., Aptel,N., Jacquet,C., Drewell,R.A., Dandolo,L., Surani,M.A., Cathala,G. *et al.* (2006) The 3' portion of the mouse *H19* Imprinting-Control Region is required for proper tissue-specific expression of the *Igf2* gene. *Cytogenet. Genome Res.*, **113**, 230–237.
28. Weber,M., Milligan,L., Delalbre,A., Antoine,E., Brunel,C., Cathala,G. and Forné,T. (2001) Extensive tissue-specific variation of allelic methylation in the *Igf2* gene during mouse fetal development: relation to expression and imprinting. *Mech. Dev.*, **101**, 133–141.
29. Leighton,P.A., Ingram,R.S., Eggenschwiler,J., Efstratiadis,A. and Tilghman,S.M. (1995) Disruption of imprinting caused by deletion of the *H19* gene region in mice. *Nature*, **375**, 34–39.
30. Reik,W., Constancia,M., Dean,W., Davies,K., Bowden,L., Murrell,A., Feil,R., Walter,J. and Kelsey,G. (2000) *Igf2* imprinting in development and disease. *Int. J. Dev. Biol.*, **44**, 145–150.
31. Davies,K., Bowden,L., Smith,P., Dean,W., Hill,D., Furuumi,H., Sasaki,H., Cattanach,B. and Reik,W. (2002) Disruption of mesodermal enhancers for *Igf2* in the minute mutant. *Development*, **129**, 1657–1668.
32. Ishihara,K., Hatano,N., Furuumi,H., Kato,R., Iwaki,T., Miura,K., Jinno,Y. and Sasaki,H. (2000) Comparative genomic sequencing identifies novel tissue-specific enhancers and sequence elements for methylation-sensitive factors implicated in *Igf2*/*H19* imprinting. *Genome Res.*, **10**, 664–671.
33. Latos,P.A. and Barlow,D.P. (2009) Regulation of imprinted expression by macro non-coding RNAs. *RNA Biol.*, **6**, 100–106.
34. Lopes,S., Lewis,A., Hajkova,P., Dean,W., Oswald,J., Forné,T., Murrell,A., Constancia,M., Bartolomei,M., Walter,J. *et al.* (2003) Epigenetic modifications in an imprinting cluster are controlled by a hierarchy of DMRs suggesting long-range chromatin interactions. *Hum. Mol. Genet.*, **12**, 295–305.
35. Arney,K.L. (2003) *H19* and *Igf2*-enhancing the confusion? *Trends Genet.*, **19**, 17–23.
36. Qiu,X., Vu,T.H., Lu,Q., Ling,J.Q., Li,T., Hou,A., Wang,S.K., Chen,H.L., Hu,J.F. and Hoffman,A.R. (2008) A complex deoxyribonucleic acid looping configuration associated with the silencing of the maternal *Igf2* allele. *Mol. Endocrinol.*, **22**, 1476–1488.
37. Leighton,P.A., Saam,J.R., Ingram,R.S., Stewart,C.L. and Tilghman,S.M. (1995) An enhancer deletion affects both *H19* and *Igf2* expression. *Genes Dev.*, **9**, 2079–2089.
38. Dekker,J. (2006) The three 'C' s of chromosome conformation capture: controls, controls, controls. *Nat. Methods*, **3**, 17–21.
39. Forne,T., Oswald,J., Dean,W., Saam,J.R., Bailleul,B., Dandolo,L., Tilghman,S.M., Walter,J. and Reik,W. (1997) Loss of the maternal *H19* gene induces changes in *Igf2* methylation

in both *cis* and *trans*. *Proc. Natl Acad. Sci. USA*, **94**, 10243–10248.
40. Zhu,X., Ling,J., Zhang,L., Pi,W., Wu,M. and Tuan,D. (2007) A facilitated tracking and transcription mechanism of long-range enhancer function. *Nucleic Acids Res.*, **35**, 5532–5544.
41. Charalambous,M., Menheniott,T.R., Bennett,W.R., Kelly,S.M., Dell,G., Dandolo,L. and Ward,A. (2004) An enhancer element at the *Igf2/H19* locus drives gene expression in both imprinted and non-imprinted tissues. *Dev. Biol.*, **271**, 488–497.